An extended X-ray absorption fine structure study of bis(μ-oxo) bridged dinuclear manganese co-ordination compounds containing alkali- and alkaline-earth-metal cations in a crown ether moiety †

Sandra Turconi,[a] Colin P. Horwitz,*,[b] Yangzhen Ciringh,[b] Susan T. Weintraub,[d] Joseph T. Warden,[c] Jonathan H. A. Nugent[a] and Michael C. W. Evans *,[a]

[a] Department of Biology, University College London, Gower St., London, UK WC1E 6BT
[b] Department of Chemistry, Carnegie Mellon University, Pittsburgh, PA 15213-3890, USA
[c] Department of Chemistry, Rensselaer Polytechnic Institute, Troy, NY 12180-3590, USA
[d] Department of Biochemistry, The University of Texas Health Science Center, San Antonio, TX 78284, USA

An X-ray absorption spectroscopic study was made of seven different manganese co-ordination compounds, six of which are dinuclear and contain the structural bis(μ-oxo) unit. In all the compounds each manganese is ligated by one crown ether Schiff-base moiety. Alkali- or alkaline-earth-metal cations were introduced into this crown ether moiety in dinuclear complexes, bringing the cations (Na^+, K^+, Ca^{2+} and Ba^{2+}) into the vicinity (<4 Å) of the manganese. The position of the X-ray absorption edge follows the order expected for the different oxidation states of manganese: 6551.6 eV for a manganese(III) monomer, 6552.1 eV for a $Mn^{III}Mn^{IV}(\mu\text{-O})_2$ dimer and 6553.5 eV for a manganese(IV) dimer. Analysis of the extended X-ray absorption fine structure of the compounds yielded information about the immediate ligation to manganese. The first shell consists of light atoms (O/N) and is composed of two sub-shells, with average distances of 1.9 Å and 2.3 Å from the Mn. The dinuclear compounds clearly show the characteristic 2.7 Å Mn−Mn distance. In the cation-containing compounds a manganese–metal distance of approximately 3.6 Å is found. The introduction of Ba^{2+} in the crown ether moiety induces substantial changes in the ligation pattern of the light elements. The properties of the compounds provide a model for discussion of the properties of the photosynthetic manganese complex, and the role and position of the Ca^{2+} cofactor.

Photosynthetic water oxidation is a process carried out by Photosystem II, PS II, a membrane-bound pigment–protein complex found in plants and cyanobacteria. Four electrons are removed from two water molecules to produce molecular oxygen. Since the process is driven by a single photon/electron charge separation event in the reaction centre of PS II, the water oxidation complex must be able to accumulate four charge equivalents. It was postulated [1,2] that the complex cycles through five oxidation states, labelled S_n, $n = 0$–4, with oxygen being evolved as S_4 is converted into S_0.

A manganese complex, most probably containing a cluster of four manganese atoms,[3] is thought to be responsible for electron abstraction and/or charge accumulation leading to water oxidation. This cluster, together with cofactors such as Ca^{2+}, Cl^- and amino acids from the surrounding protein, is termed the water oxidation complex of PS II. Despite extensive spectroscopic studies using a wide variety of techniques, many basic questions concerning its structure and function remain unanswered. Studies of the structure are hampered by the lack of PS II crystals of X-ray-diffraction quality. The only method giving direct structural information about this complex is extended X-ray absorption fine structure (EXAFS) spectroscopy. In addition, X-ray absorption spectroscopy provides information about the oxidation state of the absorbing metal (XANES, X-ray absorption near edge structure).[4,5] Many other spectroscopies have proven useful in providing complementary data. Our present understanding of the structure of the water oxidation complex can be summarised as follows: two 2.7 Å Mn−Mn interactions, together with a short manganese–light

atom distance of 1.85 Å, characteristic of two bis(μ-oxo) bridged manganese dimers, present in all reported EXAFS data.[6–8] Another shell of light atoms is often required for the fit, with a distance from Mn ranging from 1.9 to 2.3 Å.[7,9–16] This shell represents the terminal first-shell ligands to the manganese (not participating in the μ-oxo bridge). In addition to these shells for which there is general agreement, a third ligand shell at >3 Å has been described. It is best fitted with a manganese–metal interaction but the reported distances as well as the interpretations differ: (1) a single Mn [10,14] or Ca^{2+} ion [12] at 3.3 Å; (2) a single Ca^{2+} ion at 3.7 Å;[9,17] or (3) a combination of both manganese and calcium at 3.3 Å;[6,10] and, most recently, (4) a Ca^{2+} ion at 3.4–3.5 Å.[18]

The reaction of manganese(II) co-ordination compounds with molecular oxygen is still a relatively unexplored area.[19–21] It is known that some manganese(II) compounds induce cleavage of the O=O double bond producing oxo-bridged dimers, $Mn^{III}_2(\mu\text{-O})$ and $Mn^{IV}_2(\mu\text{-O})_2$ complexes, and larger clusters. If one understands how the O=O bond cleavage process proceeds, then by the principle of microscopic reversibility insights are gained as to how O_2 might be derived from H_2O in the water oxidation complex of PS II. In general, however, the formation pathway to these compounds is not well understood and small changes in reaction conditions can lead to quite different complexes. For example, we have observed incomplete oxygen-transfer reactions [22,23] from bis(μ-oxo) dimers to manganese(II) monomers leading to tri- or tetra-metallic oxo-containing clusters when the dimer and the manganese(II) monomer are both soluble in the reaction medium.[24] In contrast, when the dimer precipitated during the reaction, pure bis(μ-oxo) dimer was isolated. The larger clusters may be relevant, at least from a structural point of view, to the tetramanganese water oxidation complex,[25–27] while the dimers are interesting because they catalyse the important H_2O_2 disproportionation reaction.[28–30]
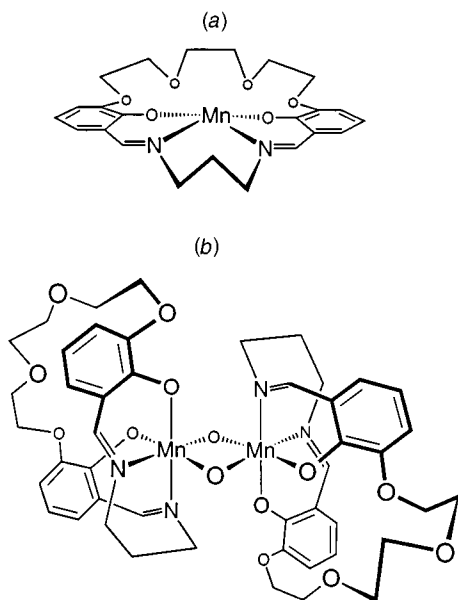
Fig. 1 Structural representations of the manganese co-ordination compounds studied (*a*) [Mn^{III}(SALPN)]PF$_6$, (*b*) [{Mn^{IV}(SALPN)-(μ-O)}$_2$]. The two crown ether moieties in (*b*) can each contain one alkali/alkaline-earth-metal cation (Na$^+$, K$^+$, Ca^{2+} or Ba^{2+})

In this study we have characterised, by means of EXAFS and XANES spectroscopies, seven different manganese complexes containing crown ether moieties as a portion of the ligand structure. Schematic representations of the mononuclear manganese(III) and dinuclear Mn$^{IV}_2$(μ-O) compounds used in this study are shown in Fig. 1. The manganese(III) centre is ligated by the 3,3′-17-crown-6-SALPN ligand (referred to as SALPN throughout for brevity) in what is assumed to be the typical square-planar geometry found for other manganese(III) Schiff-base complexes,[31] Fig. 1(*a*). In contrast, the manganese(IV) dimer is presumed to have the ligand in the *cis*-β configuration, as found for the [{Mn^{IV}(SALPN)(μ-O)}$_2$] analogue,[32,33] Fig. 1(*b*). We have shown[34] that the dimer readily incorporates alkali- and alkaline-earth-metal cations into the crown ether portion of the ligand and in this study we have found that the cations are close (<4 Å) to the manganese centres. Every crown ether moiety incorporates a single cation, so that a 1:1 stoichiometry to Mn is maintained in all the compounds. In addition to the Mn$^{IV}_2$(μ-O)$_2$ dimer compounds, a mixed-valent Mn^{III}Mn^{IV}(μ-O)$_2$ compound containing Ba^{2+} as the cation in the crown ether moieties was studied. For simplicity we will use the following names for the compounds shown in Fig. 1: (*a*), Mn(SALPN); (*b*), bis(μ-oxo) or bis(μ-oxo)·2Y (Y = Na$^+$, K$^+$, Ca^{2+} or Ba^{2+}). Unfortunately, we were not able to produce a bis(μ-oxo) compound with Sr^{2+} present in the crown ether moiety. These compounds were judged to be good models for the manganese cluster of the water oxidation complex and a comparison was made of the structural parameters and oxidation states of the complex and the model compounds.

Results

Synthesis of the cation-free Mn$^{IV}_2$(μ-O)$_2$ dimer involved oxidation of the manganese(II) form with O$_2$ in CH$_3$CN. This reaction was complete within approximately 5 min. The dimer precipitated from solution and was isolated in 80–90% yield. This procedure, which is a straightforward adaption of a method used to prepare Schiff-base bis(μ-oxo) dimers not possessing the pendant crown ether group,[24] relies on the low solubility of the dimer to prevent subsequent intermetal oxygen transfer reactions with unoxygenated Mn^{II}. Insertion of the alkali- and alkaline-earth-metal cations proceeds smoothly upon addition of 2 molar equivalents of the appropriate salt to a slurry of the

Table 1 Positions of the X-ray absorption edge of the manganese compounds

Compound	Oxidation state	Edge position/eV
Mn(SALPN)	III	6551.6
bis(μ-oxo)	IV, IV	6553.5
bis(μ-oxo)·2Na$^+$	IV, IV	6553.4
bis(μ-oxo)·2K$^+$	IV, IV	6553.7
bis(μ-oxo)·2Ca^{2+}	IV, IV	6553.7
bis(μ-oxo)·2Ba^{2+}	IV, IV	6553.2
bis(μ-oxo)·2Ba^{2+}	III, IV	6552.1

The location of the first inflection point was determined as the maximum of the first derivative of the edge region (6440–6560 eV). Energy calibration was based on the position of the sharp pre-edge peak of KMnO$_4$ at 6543.3 eV. No smoothing or filtering functions were applied. The monochromator resolution was 0.1 eV. Estimated error maximum ±0.2 eV.

dimer in CH$_3$CN. The one mixed-valent compound examined in this study was prepared by reduction of bis(μ-oxo)·2Ba^{2+} with [Fe(η-C$_5$Me$_5$)$_2$] in CH$_3$CN and then the solvent was removed *in vacuo*. After redissolving the reduced dimer in CH$_2$Cl$_2$ it was precipitated by the addition of light petroleum (b.p. 40–60 °C). Electrochemical measurements showed no evidence for [Fe(η-C$_5$Me$_5$)$_2$] or [Fe(η-C$_5$Me$_5$)$_2$]$^+$ in the sample.

The values of the manganese K-edge energies of the compounds are given in Table 1. The value for the Mn(SALPN) compound, containing Mn^{III}, is 6551.6 eV, while for the Mn^{IV}-containing compounds the average value is 6553.5 eV. The edge energy of the only Mn^{III}Mn^{IV} compound is intermediate between those two, at 6552.1 eV.

Raw EXAFS data and the respective Fourier transforms for Mn(SALPN), bis(μ-oxo) and bis(μ-oxo)·2Y compounds are shown in Fig. 2. The Fourier-filtered data together with the corresponding fits are shown in Fig. 3. The full parameter sets for the fits to the Mn(SALPN) and bis(μ-oxo) compounds are given in Table 2. The first peak in the Fourier transforms, at approximately 1.9 Å, represents light atoms directly bound to manganese. It is composed of two sub-shells, which consist of oxygen and nitrogen atoms. The shell was modelled with nitrogen being responsible for the sub-shell at the longer distance. However, it must be stressed that EXAFS cannot distinguish between the elements of similar atomic number. This peak is narrower and centred at slightly longer distances for Mn-(SALPN) as compared to the compounds with the bis(μ-oxo) core. For the latter the two sub-shells are wider apart, with the first distance shortening to 1.86 Å [compared to 1.94 Å in Mn(SALPN)] and the second lengthening to 2.36 Å [2.3 Å in Mn(SALPN)]. The bis(μ-oxo)·2Ba^{2+} compound shows a completely changed environment in the first shell of ligands: the two sub-shells are even wider apart and are resolved separately, due to a drastic shortening of the distance of the first interaction to 1.69 Å. The stoichiometry of the co-ordination is changed as well. The second peak in the Fourier transform of Mn(SALPN) is very broad and it also consists of two sub-shells of light atoms, at distances of 2.92 and 3.29 Å. In the compounds with the bis(μ-oxo) core the interactions contributing to this peak are resolved into two separate peaks or a peak and a shoulder. The shorter of the two interactions, ≈2.7 Å, represents the Mn−Mn interaction while the longer originates from a shell of light atoms in the bis(μ-oxo) compound at 3.24 Å. In the bis(μ-oxo)·2Y compounds this longer shell is best fitted with the manganese–metal cation interaction and its distance is increased to ≈3.6 Å. One more shell of light atoms can be fitted at longer distances, 3.8–4.1 Å. The fit containing five shells is still significant, as can be seen from the number of independent points in the data (see Table 2).

In all the compounds containing a bis(μ-oxo) core mentioned above both manganese centres were in the +4 oxidation state. In addition to these, we studied a mixed-valent Mn^{III}Mn^{IV}(μ-
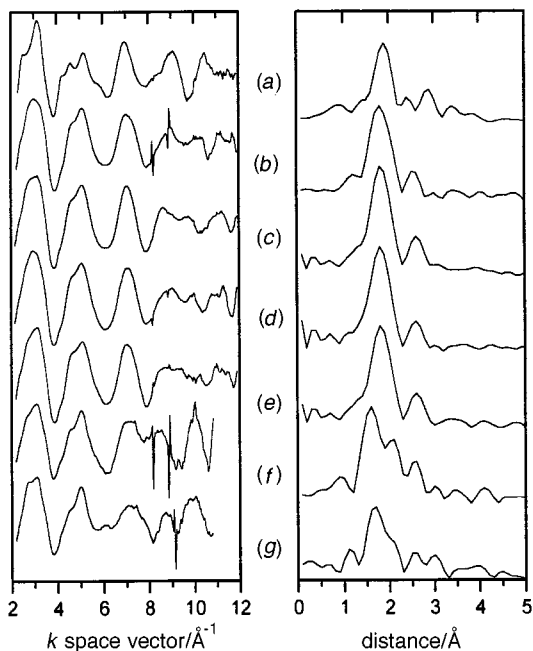
Fig. 2 Background-subtracted, k^3-weighted raw EXAFS data (left) and Fourier transforms (right) for (*a*) Mn(SALPN), (*b*) bis(μ-oxo), (*c*) bis(μ-oxo)·2Na⁺, (*d*) bis(μ-oxo)·2K⁺, (*e*) bis(μ-oxo)·2Ca²⁺, (*f*) bis(μ-oxo)·2Ba²⁺ and (*g*) MnᴵᴵᴵMnᴵⱽbis(μ-oxo)·2Ba²⁺ compounds. The *y* axes for all the Fourier transforms are uniformly scaled (maximum 1.1)
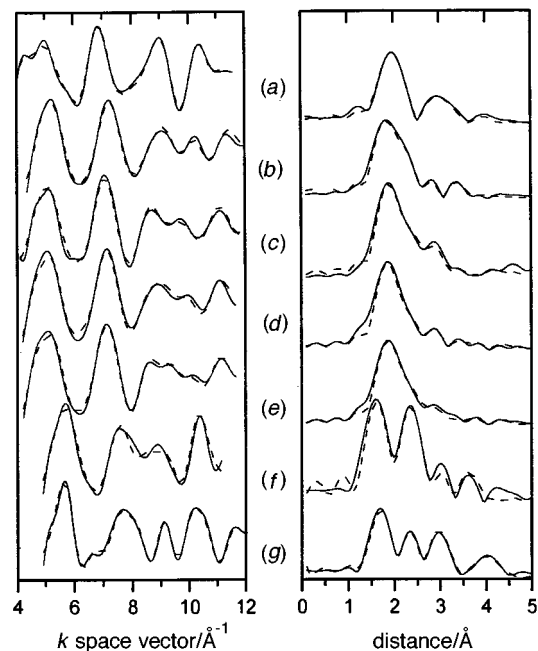
Fig. 3 Fits to Fourier-filtered k^3-weighted EXAFS data (left) and corresponding Fourier transforms (right) for (*a*) Mn(SALPN), (*b*) bis(μ-oxo), (*c*) bis(μ-oxo)·2Na⁺, (*d*) bis(μ-oxo)·2K⁺, (*e*) bis(μ-oxo)·2Ca²⁺, (*f*) bis(μ-oxo)·2Ba²⁺ and (*g*) MnᴵᴵᴵMnᴵⱽbis(μ-oxo)·2Ba²⁺ compounds. The continuous line represents experimental data and the dashed line the fitted model. For fitting parameters see Table 2. The *y* axes for the Fourier transforms have been uniformly scaled to allow direct comparison

O)₂ compound with Ba²⁺ in the crown ether moiety. The raw EXAFS data and its Fourier transform for this compound are shown at the bottom of Fig. 2, while the Fourier-filtered data, their Fourier transforms and the theoretical fits are displayed in the lower part of Fig. 3. Again, as for the Mnᴵⱽ₂(μ-O)₂ compound, the immediate manganese ligands are resolved in two shells, the first of which is at a very short distance of 1.72 Å. The intensities of the first two peaks indicate a smaller number of ligands in the first shell. The third peak, at 2.94 Å, represents the Mn–Mn interaction. As compared to the Mnᴵⱽ₂ compound, Ba²⁺ is, at 4 Å, more distant from the manganese while the shell of light atoms has moved closer, to 3.9 Å from the Mn. The fit parameters for the MnᴵᴵᴵMnᴵⱽbis(μ-oxo)·2Ba²⁺ compound are given at the right-hand side of Table 2.

The data in Table 2 show that the distances between Mn and alkali/alkaline-earth-metal cations vary around 3.6 Å for the bis(μ-oxo)·2Y compounds, which is similar to the distance reported for a manganese–metal interaction in PS II, where the metal could be Mn or Ca²⁺. In order to test for the sensitivity of EXAFS to the ligand type, we carried out a fit in which manganese was assumed to be responsible for the 3.6 Å interaction in the bis(μ-oxo)·Ca²⁺ compound. The fit to the Fourier-filtered isolate of this shell assuming one Ca²⁺ has a fit index (FI) 8% better than that with one manganese.

Discussion

XANES

The position of the X-ray absorption edge is characteristic of the absorbing element, and within a few eV of its oxidation state and the electron density distribution. Owing to the latter, it is not possible to make straightforward comparisons of oxidation state between complexes with different ligation to the same central ion. The compounds studied here exhibit the same ligation pattern to the Mn. As can be seen in Table 1, the most obvious change in the position of the X-ray absorption edge, of approximately 2 eV, is found between the values for Mn(SALPN) and bis(μ-oxo)·2Y compounds. This is easily explained by the difference in the oxidation state of the Mn atoms in these compounds (Mnᴵᴵᴵ and Mnᴵⱽ₂, respectively). The introduction of the metal cation in the crown ether moiety has little effect on the

position of the edge for the bis(μ-oxo) compounds. These variations are small (almost on the limit of the experimental error) and do not seem to show a clear tendency. The bis(μ-oxo) MnᴵᴵᴵMnᴵⱽ compound shows an intermediate edge position as compared to Mn(SALPN) (Mnᴵᴵᴵ) and bis(μ-oxo)·2Ba²⁺ (Mnᴵⱽ₂). This fits well with the proposal that the 1e⁻ oxidation of Mn results in an approximately 2 eV shift of the absorption edge for mononuclear manganese compounds,[35] while for complexes containing multiple Mn atoms the edge position reflects the average redox state and is influenced by the nuclearity of the complex (see discussion in ref. 36).

EXAFS of the Mn(SALPN), bis(μ-oxo) and bis(μ-oxo)·2Y compounds

Raw EXAFS data for Mn(SALPN), bis(μ-oxo) and bis(μ-oxo)· 2Y (Fig. 2) show a remarkable lack of features beyond 3 Å. This might be a consequence of a compact Mn₂O₂ core due to the bis(μ-oxo) bridge and therefore overlapping of different interactions leading to fewer, broad peaks. Fourier-filtered data and the best fits are shown in Fig. 3, while the parameters of the fits are summarised in Table 2.

The first two shells can be seen as separate in the Fourier transforms of the raw data (Fig. 2), while they appear as a single broad peak in the Fourier-filtered data, Fig. 3. From the distances of 1.9 and 2.3 Å it is clear that these shells represent the oxygen and nitrogen atoms directly bound to manganese. The assignment of the distance of 1.9 Å to oxygen and 2.3 Å to nitrogen is purely arbitrary, for reasons described above. All of these shells should strictly be considered as originating from O, N or C or their combination. However, the position of the first peak in the Fourier transforms at the distance of 1.9 Å is likely to correspond to a Mnᴵⱽ–O distance, as nitrogen is known to build longer bonds[37–39] and may therefore be assigned to the 2.3 Å distance. The variation in bond length for O/N atoms bound to a Mn in oxidation state +4, as in bis(μ-oxo) compounds, would be expected to be of the order of 0.1 Å (1.85 *vs.* 1.95 Å). The significantly larger difference here is most likely due to distortions in the octahedral geometry of ligand binding. The

Table 2   The EXAFS fit parameters for the MnL bis(μ-oxo) and bis(μ-oxo)·2Y compounds

	Mn(SALPN)			bis(μ-oxo)			bis(μ-oxo)·Na⁺			bis(μ-oxo)·K⁺			bis(μ-oxo)·Ca²⁺			bis(μ-oxo)·Ba²⁺ Mn$^{IV, IV}$			Mn^{III}Mn^{IV}		
Shell	Atoms	r/Å	α	Atoms	r/Å	α	Atoms	r/Å	α	Atoms	r/Å	α	Atoms	r/Å	α	Atoms	r/Å	α	Atoms	r/Å	α
1	4O	1.94	0.011	4O	1.84	0.012	4O	1.88	0.010	4O	1.86	0.010	4O	1.87	0.010	4O	1.69	0.009	2O	1.72	0.005
2	3N	2.30	0.005	3N	2.34	0.007	3N	2.37	0.007	2N	2.36	0.006	2N	2.36	0.002	6N	2.28	0.005	3N	2.28	0.007
3	4O	2.92	0.009	0.5Mn	2.66	0.011	0.5Mn	2.77	0.002	0.5Mn	2.75	0.007	0.5Mn	2.77	0.005	0.5Mn	2.62	0.002	1Mn	2.94	0.003
4	4C	3.29	0.006	4O	3,24	0.011	1Na	3.55	0.025	1K	3.71	0.009	1Ca	3.63	0.013	1Ba	3.59	0.002	6O	3.93	0.010
5	2O	3.81	0.010	4C	3.59	0.008	2O	4.15	0.017	2O	4.18	0.010	2O	4.18	0.004	6O	4.04	0.007	1Ba	4.05	0.013
FI	0.12 × 10⁻³			0.2 × 10⁻³			0.2 × 10⁻³			0.3 × 10⁻³			0.2 × 10⁻³			0.3 × 10⁻³			0.21 × 10⁻³		
R	10.8			13.7			16.1			18.8			15.4			17.1			13.5		
N_i	14.6			14.5			17.0			16.9			16.9			17.1			17.6		
ε_v^2	0.88 × 10⁻⁶			1.51 × 10⁻⁵			1.04 × 10⁻⁶			2.50 × 10⁻⁶			1.61 × 10⁻⁶			2.17 × 10⁻⁶			1.45 × 10⁻⁶		

Fitting was carried out on the data Fourier filtered in a k space window of 3.5–11.5 Å⁻¹. Estimated errors: for the distances ±0.02 Å for the first and ⩽2% for the other shells; co-ordination numbers ± 30% for the first shell, up to 40–50% for the last; Debye–Waller factors ±30%. The parameters describing the goodness of the fit are defined in the Experimental section.

values are very similar to ones reported for manganese complexes whose structure was determined by X-ray crystallography,[40–43] with two (axial) manganese–ligand bonds being longer than the other, at 2.15–2.30 Å. The distance of the first shell is most probably an average between the shorter μ-oxo bridge oxygen (usually about 1.80 Å), the other oxygens (1.85 Å) and nitrogen (1.9–2.0 Å). The Debye–Waller factors for this shell are slightly higher than expected which most probably reflects the spread of distances. Bearing in mind the limitations of EXAFS (up to 30% error in co-ordination number), the number of ligands to each manganese in the first two shells totals to six, in agreement with the structure in Fig. 1(*b*).

The effect of the manganese oxidation state on the bond length for the first sub-shell of ligands is clearly visible in Table 2. The Mn−O distance for bis(μ-oxo)·2Ba^{2+} compounds can be directly compared: the 1.72 Å distance for the Mn^{III}Mn^{IV} compound is shortened to 1.69 Å in the Mn$^{IV}_2$ compound which is in agreement with a higher oxidation state.[25] Although the accepted precision limit for distances is ±0.02 Å, the statistical error of the fit of ±0.002 suggests that this difference in bond lengths may be significant.

The second peak in the EXAFS of the bis(μ-oxo) compounds is described very well by a Mn–Mn separation of 2.7 Å. This distance agrees very well with the values determined in crystallographic studies of other bis(μ-oxo) bridged manganese co-ordination compounds.[33,42–44] The fact that the number of Mn−Mn interactions is best approximated with 0.5 is in agreement with the molecule containing a single Mn−Mn distance (both centres detect the same interaction), see refs. 9, 11 and 45. This distance is subject to slight changes upon the introduction of a metal cation in the crown ether moiety. In the bis(μ-oxo)·2Y compounds the Mn−Mn distance is consistently greater by 0.1 Å than in the cation-less bis(μ-oxo) compound. The only exception to this is bis(μ-oxo)·2Ba^{2+}, which shows further important distinctions to the others and will be discussed in more detail below.

The third peak in the Fourier transforms in Fig. 3 is modelled by two shells of light atoms (4 O at 3.24 Å and 4 C at 3.59 Å) in case of the bis(μ-oxo) compound. The third peak is shifted somewhat to the longer of these two distances in the bis(μ-oxo)·2Y compounds and best modelled with a single alkali- or alkaline-earth-cation. In most of the Fourier transforms there is a small peak or shoulder still visible at approximately 3.3 Å. While this feature can be fitted with a shell of light atoms, it results in an overdetermined fit (the number of parameters is too many for the number of points) and so it was not included in the model. Although the amplitude of the third peak in the Fourier transforms is small, its significance becomes clear when fits without this shell are analysed. Both the parameters, FI and ε$_v$², clearly deteriorate (30–110%) when the manganese–cation interaction is omitted from the fit. The ε$_v$² parameter accounts for the changes in the ratio of the number of variable parameters *vs.* the number of independent points for these fits (see Experimental section).

All of the bis(μ-oxo) compounds, except bis(μ-oxo)·2Ba^{2+}, have a fourth, final shell that could be fitted with two oxygen atoms at 4.2 Å. The bis(μ-oxo)·2Ba^{2+} dimer has a higher number of light atoms that seem to contribute to this shell and the shell is at a slightly shorter distance (4.0 Å). When a model without this last shell of light atoms was fitted to the data the quality of the fit decreased by 10%, indicating that this shell is significant.

The Mn$^{IV}_2$bis(μ-oxo)·2Ba^{2+} compound shows important departures from the ligation pattern common for other bis(μ-oxo)·2Y compounds (Table 2). The first shell shows a clearly greater number of ligands at the 2.3 Å distance (six instead of two). A determination of the co-ordination number by EXAFS has a substantial error, but the increase in intensity of the second peak in the Fourier transforms (Fig. 3) is obvious, and can only be accounted for by an increased co-ordination number,

since the values of the Debye–Waller factors are comparable (see Table 2). This distance (2.3 Å) is very short and implies direct binding to manganese. Since it is difficult to imagine such a large number of ligands being directly co-ordinated to manganese, this increase in co-ordination number might be explained with a part of the second shell of light ligands being positioned closer to the manganese. However, the Debye–Waller factor is reasonably small, indicating a fairly ordered shell. Therefore, a potential explanation might be that Ba^{2+} binds to multiple water molecules possibly bringing them close to the Mn$_2$O$_2$ core. This behaviour may be related to the high co-ordination numbers that are often found for barium compounds. Combustion analysis of the bis(μ-oxo)·2Ba^{2+} compound is consistent with five water molecules per dimer.[34] Another very important difference in the first shell of bis(μ-oxo)·2Ba^{2+} as compared to other bis(μ-oxo)·2Y compounds is the surprisingly short first Mn−O interaction of 1.69 Å, visible in Fig. 3 as a clear shift of the first peak in the Fourier transforms to shorter distances. This indicates that a substantial alteration in the nature of the bonding of the very first shell of ligands has occurred. The value of 1.69 Å is identical to that reported by an EXAFS study of a different manganese-model compound,[46] and which was assigned to a Mn=O interaction.

In addition to the bis(μ-oxo)·2Y compounds discussed above which contained both manganese atoms in the +4 oxidation state, a heterovalent dimer was investigated, with a Mn^{III}Mn^{IV} core and a Ba atom in the crown ether moiety. Both the raw and Fourier-filtered EXAFS show significant differences from those of the other bis(μ-oxo) compounds and these are highlighted by comparison of the fitting parameters in Table 2. As in the case of the Mn$^{IV}_2$ compound, the two sub-shells representing the ligands directly bound to Mn are split into two distinct peaks in the Fourier transform. The distance of the first sub-shell (1.72 Å) is very short, compared to the normal Mn^{III}– or Mn^{IV}–O bond length, indicating a considerable change in the type of bond between Mn and its immediate ligands. However, a comparison of the Mn$^{IV}_2$bis(μ-oxo)·2Ba^{2+} and Mn^{III}Mn^{IV}bis(μ-oxo)·2Ba^{2+} complexes reveals a 0.03 Å increase in the bond length in this first sub-shell. It is likely that this is a significant increase because bond lengthening would be expected to occur upon reduction of the dimer. A further distinct feature of the EXAFS of the Mn^{III}Mn^{IV}bis(μ-oxo)·2Ba^{2+} compound is the lower co-ordination numbers for both the sub-shells of the first shell of ligands, compared to those of the Mn$^{IV}_2$bis(μ-oxo)·2Ba^{2+} compound. This could be explained by the reduced charge of the mixed-valent dimer, causing a loss of some water molecules. This is also clearly visible in the intensities of the first two peaks in the Fourier transforms (Fig. 3) which are almost halved as compared to those of the Mn$^{IV}_2$bis(μ-oxo)·2Ba^{2+} compound. The third shell which originates from the Mn−Mn interaction is at a considerably longer distance, 2.94 Å. The effect of the sequential protonation of the bis(μ-oxo) oxygens on the Mn−Mn distance was studied by EXAFS[47] in [{Mn^{IV}(SALPN)(μ-OH)}$_2$][CF$_3$SO$_3$]$_2$ and a Mn−Mn distance of 2.93 Å was reported for the bis(μ-oxo) bridge in which both the oxygens were protonated. However, the charge structure of the Mn^{III}Mn^{IV}bis(μ-oxo)·2Ba^{2+} compound makes it unlikely that protonation could occur. The Fourier-transfer peak corresponding to this shell is apparently more intense than in the other bis(μ-oxo)·2Y compounds. This enhanced intensity might be only a relative change, caused by the lower intensity of the first two peaks. However, attempts to fit this shell with 0.5 Mn–Mn interactions resulted in negative Debye–Waller factors. The longer distance and lower co-ordination number seem to indicate a change in the manganese core structure. Another characteristic of this compound is the longer distance of the Ba^{2+} cation to the Mn, at 4 Å. All these features seem to indicate that the structure of the Mn^{III}Mn^{IV}bis(μ-oxo)·2Ba^{2+} compound is somewhat less compact than that of the other dinuclear manganese compounds studied here.

Comparison with Photosystem II

In the view of our present knowledge of the structure of the manganese cluster of PS II the compounds with the bis(μ-oxo) core examined here are directly relevant as structural models. The present study reveals several features common to both. First, the distance of the first shell of light elements to Mn and, more interestingly, the fact that the first shell is split into two sub-shells are both very similar to the behaviour of PS II (see Introduction). This splitting of the first ligand shell is most probably due to an octahedral geometry for Mn in which the two bridging oxygens provide the shortest bonds, the two other, in-plane ligands somewhat longer bonds (especially if they are nitrogen) and the two axial ligands the longest first shell bonds (2.2–2.3 Å) (for a typical crystal structure, see Palaskin et al.[43]) resulting in the reported bond-length spread. Secondly, the Mn−Mn distance of approximately 2.7 Å as a characteristic of the bis(μ-oxo) structural motif is present in both the model compounds and PS II. This indicates that the immediate surroundings of the manganese centres are quite similar in both cases, which could imply a similar electron density distribution and allow for edge-position comparisons. The positions of the absorption edge for the Mn^{IV}_2 compounds agree surprisingly well with those reported for manganese in the S_2 state of the water oxidation complex of PS II.[48] On the other hand, the edge position of the manganese(III) compound [Mn(SALPN)] is in very good agreement with that of the S_1 state of the water oxidation complex.[17,48] This could imply that the $S_1 \longrightarrow S_2$ transition involves oxidation-state changes of two or more of the four Mn atoms in the water oxidation complex, which is difficult to reconcile with our knowledge of the water oxidation process, in which each S state transition reflects a single electron transfer. However, it should be noted that the reported edge position values for the S_1 and S_2 states have varied considerably: Klein and co-workers have reported values ranging from 6550.4 eV to 6551.7 eV for S_1 and 6552.2–6553.5 eV for S_2.[49–52] Our results show less variation: 6551.6–6551.8 eV for S_1, and 6552.6–6553.6 eV for S_2.[17,48] Low values of 6550.2 eV for S_1 and 6551.2 eV for S_2 were reported by Ono et al.[53]

It is known that at least one Ca^{2+} is present in the vicinity of the PS II manganese cluster. However, considerable uncertainty exists about its probable distance from the Mn (see Introduction). Two recent studies highlight the uncertainties connected with detecting the Ca^{2+} contribution, both based on the replacement of Ca^{2+} with an element with a larger atomic number (Sr or Tb), making it easily detectable in EXAFS. However, quite different conclusions were reached: Latimer et al.[18] determined a Mn−Ca^{2+} distance of 3.46 Å, while Hatch et al.[16] and Riggs-Gelasco et al.[8] inferred that there was no Mn−Ca^{2+} interaction at distances shorter than 4 Å. One aspect of this problem is that EXAFS cannot distinguish between elements with similar atomic number. Another Mn atom ($Z = 25$) at a distance of >3 Å would be very difficult to distinguish from a Ca ($Z = 20$).

The manganese–cation distances found for the model compounds in this study are very similar to that proposed for PS II, so we decided to determine to what degree this limitation is due to the method and how much is due to the low signal-to-noise ratio of the PS II samples. Since we know that in the model compounds only one Mn−Mn interaction is present, the other manganese–metal interaction is clearly assigned to Ca [in the case of bis(μ-oxo)·$2Ca^{2+}$]. It is a significant shell, since its removal from the simulation leads to a >30 % increase in the FI. Moreover, this ≈3.6 Å peak cannot be described well with a single shell or combinations of shells of light atoms (data not shown). So, in so far as the model compound is considered, it is clear that this peak originates from Ca^{2+} and is well modelled by Ca^{2+}. The question is, would it be possible to distinguish it from a putative Mn. To address this problem, a fit (overall and of the Fourier-filtered single-shell isolate) was run, replacing

Ca^{2+} for Mn. The FI is about 8% smaller in the case of Ca^{2+}, indicating a better fit with Ca^{2+}, but only just above the limit of significance (usually considered to be 5%). This demonstrates that, even with an extremely good signal-to-noise ratio, it is difficult to make a distinction between elements with similar atomic number and that this limitation is intrinsic to EXAFS. This uncertainty is limited to elements belonging to the same row in the Periodic Table: an attempt to fit this shell with Na or Ba in the place of Ca results in an increase of more than 40% in the FI parameter, giving a clearly poorer fit.

It is well documented that the removal of the Ca^{2+} influences both functional and structural properties of the water oxidation complex.[3] There seems to be no pronounced alteration in the edge position upon cation exchange in the model compounds, while some studies of edge measurements for PS II samples that had been depleted of Ca^{2+} (effectively Na^+ substituted) report a significant decrease in edge energies[17,53] which was reversed upon reconstitution with Ca^{2+}.[53] This reversal is confirmed in an account of PS II particles reconstituted with either Ca^{2+} or Sr^{2+}, resulting in edges which were very similar to the native ones.[8,18] Furthermore, Latimer et al.[18] report an edge shift between the Ca^{2+}- and Sr^{2+}-reconstituted preparations of only 0.2 eV, similar to differences found between model compounds of the bis(μ-oxo) series. This would seem to indicate that the presence or absence of Ca^{2+} has a bigger impact on the manganese-core in the water oxidation complex than the cations in the above model compounds, but the exchange of cations does not lead to any structural reorganisation. This could indicate an electrostatic, rather than structural, role for Ca in the water oxidation complex: there doesn't seem too much perturbation on introducing another cation, as long as the charge is preserved, but significant change occurs with change of charge. However, in the case of the cations in the model compounds, a more structural role might be proposed, on the basis of the remarkable effect of Ba^{2+}.

Experimental

Synthesis of $[Mn^{III}(3,3'-17-crown-6-SALPN)]PF_6$ and $[\{Mn^{IV}(3,3'-17-crown-6-SALPN)(\mu-O)\}_2]$

The synthesis of the manganese(III) monomer and the $Mn^{IV}_2(\mu-O)_2$ dimer containing the 'crown-6' Schiff-base ligand and the insertion of Na^+, K^+, Ca^{2+} and Ba^{2+} into the crown ether moieties in the dimer were conducted as previously described.[34]

EXAFS Spectroscopy

The EXAFS measurements were carried out at the CLRC Daresbury Laboratory, UK. The spectra were collected in transmission mode on Station 8.1 equipped with a slitless Si(111) double-bent crystal monochromator and a toroidal focusing mirror. Ion chambers filled with an Ar–He mixture were used as detectors. The beam energy was 2 GeV with an average beam current of 150 mA. Harmonic rejection was achieved by offsetting the first monochromator crystal, while retaining 70% of the incoming beam. Energy calibration was based on the position of the sharp pre-edge peak of $KMnO_4$ at 6543.3 eV. A scan of $KMnO_4$ was recorded every 6–8 h.

The powder samples were diluted with appropriate amounts of boron nitride and mounted on tape to obtain an absorption coefficient (μ_x) between 1.5 and 2.5. Each scan lasted approximately 1 h and the samples were kept at room temperature. Three scans were taken for each compound and summed.

Data analysis

The manganese K-edge energies were determined by taking the first inflection point of the edge of absorption (maximum of the first derivative). No fitting or smoothing functions were applied.

The data were processed using programs developed at the

Daresbury Laboratory. The signal was divided by the intensity of the incoming X-ray beam (I_0) and energy calibration performed using the EXCALIB program. The background subtraction was performed employing the EXBACK program: pre-edge background was subtracted using a polynomial function of the first degree, while for the post-edge three coupled third-degree polynomials were used. Finally, the EXAFS, presented in k space and weighted by k^3, was analysed using EXCURVE 92. This program calculates the theoretical EXAFS for a given set of parameters by the application of the fast curved wave theory and the Hedin–Lindquist description of the exchange potential. The theoretical model parameters are fitted to the experimental EXAFS by a non-linear least-squares routine. The Fourier transforms of both the experimental and theoretical EXAFS functions were used for model building and visual determination of the quality of the fit. Data analysis was performed in k space, both on raw data and on data Fourier filtered by applying a window function from 0.7 to 4.5 Å. The structural models were compared using the criteria for the goodness of the fit recommended by the International Workshop on Standards and Criteria in XAFS.[54] These include the fit index, FI, defined as [7,9,54] in equation (1), the agreement fact R

$$\text{FI} = \sum_i^N 1/\sigma_i^2[\chi_{exp}(k_i) - \chi_{theor}(k_i)]^2 \qquad (1)$$

[equation (2)] and ε_v^2, a reduced χ^2 function [equation (3)],

$$R = \sum_i^N 1/\sigma_i[|\chi_{exp}(k_i) - \chi_{theor}(k_i)|] \times 100\% \qquad (2)$$

$$\varepsilon_v^2 = 1/N_{ind} - p\left(N_{ind}/\sum_i^N N\right)\sum 1/\sigma_i^2[\chi_{exp}(k_i) - \chi_{theor}(k_i)]^2 \quad (3)$$

where N_{ind} is the number of independent points [equation (4)]

$$N_{ind} = 2(r_{max} - r_{min})(k_{max} - k_{min})/\pi \qquad (4)$$

and p is the number of parameters. Different combinations of O, N and C atoms were fitted to the light atom shells. However, EXAFS is not sensitive enough to distinguish between the back-scattering amplitude from elements with very similar atomic number, Z. This is especially true for C, N and O ($Z = 6$, 7 and 8, respectively). Therefore, it can only be concluded that light atom shells consist of atoms from the first row of the Periodic Table. The co-ordination number itself is subject to up to 30–40% error. The approach adopted to fitting co-ordination numbers was to vary them systematically in steps of 1 while the Debye–Waller factors, $\alpha = 2\sigma^2$, were refined to obtain the best simulation (σ is the root mean square deviation in the interatomic distances).[7,9] The values were in a good agreement with the fits to the raw data, where co-ordination numbers were left free.

Acknowledgements

References

1 P. Joliot, G. Barbieri and R. Chabaud, *Photochem. Photobiol.*, 1969, **10**, 309.
2 B. Kok, B. Forbush and M. McGloin, *Photochem. Photobiol.*, 1970, **11**, 457.
3 R. J. Debus, *Biochim. Biophys. Acta*, 1992, **1102**, 269.
4 R. Prins, in *X-Ray Absorption: Principles, Applications, Techniques of EXAFS, SEXAFS and XANES*, eds. S. P. Cramer and D. C. Koningsberger, Wiley, New York, 1988.
5 V. K. Yachandra, *Methods Enzymol.*, 1995, **246**, 638.
6 V. K. Yachandra, V. J. DeRose, M. J. Latimer, I. Mukerji, K. Sauer and M. P. Klein, *Science*, 1993, **260**, 675.

7 D. J. MacLachlan, J. H. A. Nugent, P. J. Bratt and M. C. W. Evans, *Biochim. Biophys. Acta*, 1994, **1186**, 186.
8 P. J. Riggs-Gelasco, R. Mei, D. F. Ghanothakis, C. F. Yocum and J. E. Penner-Hahn, *J. Am. Chem. Soc.*, 1996, **118**, 2400.
9 D. J. MacLachlan, B. J. Hallahan, S. V. Ruffle, J. H. A. Nugent, M. C. W. Evans, R. W. Strange and S. S. Hasnain, *Biochem. J.*, 1992, **285**, 569.
10 V. J. DeRose, I. Mukerji, M. J. Latimer, V. K. Yachandra, K. Sauer and M. P. Klein, *J. Am. Chem. Soc.*, 1994, **116**, 5239.
11 I. Mukerji, J. C. Andrews, V. J. DeRose, M. J. Latimer, V. K. Yachandra, K. Sauer and M. P. Klein, *Biochemistry*, 1994, **33**, 9712.
12 J. E. Penner-Hahn, R. M. Fronko, V. L. Pecoraro, C. F. Yocum and N. R. Bowlby, *J. Am. Chem. Soc.*, 1990, **112**, 2549.
13 R. D. Guiles, J. L. Zimmermann, A. E. McDermott, V. K. Yachandra, J. L. Cole, L. Dexheimer, R. D. Britt, K. Weighardt, U. Bossek, K. Sauer and M. P. Klein, *Biochemistry*, 1990, **29**, 471.
14 G. N. George, R. C. Prince and S. P. Cramer, *Science*, 1989, **243**, 789.
15 R. D. Guiles, V. K. Yachandra, A. E. McDermott, J. L. Cole, S. L. Dexheimer, R. D. Britt, K. Sauer and M. P. Klein, *Biochemistry*, 1990, **29**, 486.
16 C. Hatch, M. Grush, R. Bradley, R. LoBrutto, S. Cramer and W. Frasch, in Xth International Photosynthesis Congress, Montpellier, 1995, p. 425.
17 D. J. MacLachlan, J. H. A. Nugent and M. C. W. Evans, *Biochim. Biophys. Acta*, 1994, **1185**, 103.
18 M. J. Latimer, V. J. DeRose, I. Mukerji, V. K. Yachandra, K. Sauer and M. P. Klein, *Biochemistry*, 1995, **34**, 10 898.
19 C. J. Weschler, B. M. Hoffman and F. Basolo, *J. Am. Chem. Soc.*, 1975, **97**, 5278.
20 B. M. Hoffman, C. J. Weschler and F. Basolo, *J. Am. Chem. Soc.*, 1976, **98**, 5473.
21 C. P. Horwitz and G. C. Dailey, *Comments Inorg. Chem.*, 1993, **14**, 283.
22 R. H. Holm, *Chem. Rev.*, 1987, **87**, 1401.
23 L. K. Woo, *Chem. Rev.*, 1993, **93**, 1125.
24 C. P. Horwitz, P. J. Winslow, J. T. Warden and C. A. Lisek, *Inorg. Chem.*, 1993, **32**, 82.
25 G. W. Brudvig and R. H. Crabtree, *Prog. Inorg. Chem.*, 1989, **37**, 99.
26 L. Que and A. E. True, in *Dinuclear Iron- and Manganese-Oxo Sites in Biology*, ed. S. J. Lippard, New York, 1990.
27 K. Wieghardt, *Angew. Chem., Int. Ed. Engl.*, 1989, **28**, 1153.
28 A. Gelasco, A. Askenas and V. L. Pecoraro, *Inorg. Chem.*, 1996, **35**, 1419.
29 U. Bossek, M. Saher and T. Weyherm, *J. Chem. Soc., Chem. Commun.*, 1992, 1780.
30 P. J. Pessiki, S. V. Khangulov, D. M. Ho and G. C. Dismukes, *J. Am. Chem. Soc.*, 1994, **116**, 891.
31 C. P. Horwitz, G. C. Dailey and F. S. Tham, *Acta Crystallogr., Sect. C*, 1995, **51**, 815.
32 J. W. Gohdes and W. H. Armstrong, *Inorg. Chem.*, 1992, **31**, 368.
33 E. Larson, M. S. Lah, X. Li, J. A. Bonadies and V. L. Pecoraro, *Inorg. Chem.*, 1992, **31**, 373.
34 C. P. Horwitz, J. T. Warden and S. T. Weintraub, *Inorg. Chim. Acta*, 1996, **246**, 311.
35 J. A. Kirby, D. B. Goodin, T. Wydrzynski, A. S. Robertson and M. P. Klein, *J. Am. Chem. Soc.*, 1981, **103**, 5537.
36 K. Sauer, V. K. Yachandra, R. D. Britt and M. P. Klein, in *Manganese Redox Enzymes*, ed. V. L. Pecoraro, VCH, New York, 1992.
37 K. Wieghardt, *Angew. Chem.*, 1989, **101**, 1179.
38 N. Kitajima, H. Komatsuzaki, S. Hikichi, M. Osawa and Y. Morooka, *J. Am. Chem. Soc.*, 1994, **116**, 11 596.
39 R. T. Stibrany and S. M. Gorun, *Angew. Chem., Int. Ed. Engl.*, 1990, **29**, 1156.
40 T. Noguchi, T. Ono and Y. Inoue, *Biochim. Biophys. Acta*, 1995, **1228**, 189.
41 J. B. Vincent, H.-L. Tsai, A. G. Blackman, S. Wang, P. D. W. Boyd, K. Folting, J. C. Huffman, E. B. Lobkovsky, D. N. Hendrickson and G. Christou, *J. Am. Chem. Soc.*, 1993, **115**, 12 353.
42 K. Wieghardt, U. Bossek, B. Nuber, J. Weiss, J. Bonvoisin, M. Corbella, S. E. Vitols and J. J. Girerd, *J. Am. Chem. Soc.*, 1988, **110**, 7398.
43 P. M. Palaskin, R. C. Stoufer, M. Mathew and G. J. Palenik, *J. Am. Chem. Soc.*, 1972, **94**, 2121.
44 M. Stebler, A. Ludi and H.-B. Bürgi, *Inorg. Chem.*, 1986, **25**, 4743.
45 P. J. Riggs-Gelasco, R. Mei, C. F. Yocum and J. E. Penner-Hahn, *J. Am. Chem. Soc.*, 1996, **118**, 2387.
46 K. Ayougou, E. Bill, J. M. Charnock, C. D. Garner, D. Mandom, A. X. Trutwein, R. Weiss and H. Winkler, *Angew. Chem., Int. Ed. Engl.*, 1995, **34**, 343.

47 M. J. Baldwin, T. L. Stemmler, P. J. Riggs-Gelasco, M. L. Kirk, J. E. Penner-Hahn and V. L. Pecoraro, *J. Am. Chem. Soc.*, 1994, **116**, 11 349.

48 S. Turconi, C. P. Horwitz, S. T. Weintraub, J. T. Warden, J. H. A. Nugent and M. C. W. Evans, in Xth International Photosynthesis Congress, Montpellier, 1995, p. 301.

49 V. K. Yachandra, R. D. Guiles, A. McDermott, R. D. Britt, S. L. Dexheimer, K. Sauer and M. P. Klein, *Biochim. Biophys. Acta*, 1986, **850**, 324.

50 J. Cole, V. K. Yachandra, R. D. Guiles, A. E. McDermott, R. D. Britt, S. L. Dexheimer, K. Sauer and M. P. Klein, *Biochim. Biophys. Acta*, 1987, **890**, 395.

51 W. Liang, M. J. Latimer, H. Dau, T. A. Roelofs, V. K. Yachandra, K. Sauer and M. P. Klein, *Biochemistry*, 1994, **33**, 4923.

52 T. A. Roelofs, W. Liang, M. J. Latimer, R. Cinco, A. Rompel, J. C. Andrews, V. K. Yachandra, K. Sauer and M. P. Klein, Xth International Photosynthesis Congress, Montpellier, 1995, p. 459.

53 T.-A. Ono, T. Noguchi, Y. Inoue, M. Kusunoki, H. Yamaguchi and H. Oyanagi, *FEBS Lett.*, 1993, **330**, 28.

54 F. W. Lytle, D. E. Sayers and E. A. Stern, *Physica B*, 1989, **158**, 701.